INTERNATIONAL JOURNAL FOR NUMERICAL METHODS IN FLUIDS
Int. J. Numer. Meth. Fluids 2002; **40**:487–496 (DOI: 10.1002/fld.300)

A new high-order finite volume element method with spectral-like resolution

F. Sarghini*,†, G. Coppola and G. de Felice

Department of Energetics, Thermo-Fluid Dynamics and Environmental Control, University of Naples "Federico II", P.le Tecchio 80, 80125 Naples, Italy

SUMMARY

In this work, a new high-order finite volume element method with good spatial resolution characteristics is presented. The method is based on a functional representation of the unknowns based on the finite element method, a balance of physical quantities in weak formulation obtained by using the finite volume method, and an implicit reduction of some of the unknowns obtained by enforcing functional relations between some of them. Applications to hyperbolic and elliptic operators in 1D and 2D, as well as to Navier–Stokes equations for incompressible flows are presented. Copyright © 2002 John Wiley & Sons, Ltd.

KEY WORDS: finite volume element; finite element box scheme

1. INTRODUCTION

The fulfillment of numerical requirements in specific classes of computational fluid dynamics problems can be considered still an open challenge. For example, in large eddy simulations of turbulent flows the use of standard second-order finite difference (FD) schemes cannot be considered a completely satisfying solution. Higher-order accuracy, spectral or spectral-like spatial resolution, low dispersion and low dissipation characteristics, together with the capability of describing complex geometries with reasonable computational effort are required. Recently, research was addressed to develop FD schemes partially satisfying all these requirements [1–5] which in some cases seem to be antithetical. Although the classical finite volume (FV) method is in common use as a discretization method, yet the FV approach is not fully systematic, as it requires a scheme for approximating certain fluxes, which is often done in an effective but rather ad hoc and restrictive way that depends upon truncation error analysis. The evidence of the lack of fully developed guiding principles for the FV approach rely on the lack of founding theory even though some work is present in literature [6–12]. The finite

*Correspondence to: F. Sarghini, Department of Energetics, Thermo-Fluid Dynamics and Environmental Control, University of Naples "Federico II", P.le Tecchio 80, 80125 Naples, Italy.
†E-mail: sarghini@unina.it

Received May 2001
Revised October 2001

volume element (FVE) method [13] was developed as an attempt to use finite element ideas to create a more systematic and theoretically controlled FV methodology. The FVE method was applied using triangular elements to advection and advection–diffusion problems [14, 15] and to Navier–Stokes equations [16]. More recently, Swaminathan *et al.* [17] applied the streamline upwind Petrov–Galerkin technique to FVE. Although recent advances in the FV method showed a renewed interest in mixed finite element–finite volumes formulations [19–21], higher order formulations are not very common [22]. In this paper a new FVE method is presented, coupling high accuracy and good spatial resolution characteristics, defined as the property of minimizing the number of grid points required to resolve all relevant wavelengths involved in the physical problem. The method is targeted to applications in which low dispersion and low dissipation characteristics are required.

2. METHODOLOGY FUNDAMENTALS

In order to introduce the fundamental concepts of the proposed methodology, let us consider the univariate case relative to a physical domain $\Omega \in \mathbb{R}$. We can introduce the finite element (FE) partition $\mathscr{T}_{\mathrm{FE}}$ of Ω and the dual $\mathscr{T}_{\mathrm{FV}}$ on which the conservation balance is enforced in weak form, as shown in Figure 1(a), being $\bigcup_{m=1}^{N} \mathscr{T}_{\mathrm{FE}_m} = \Omega$, $\bigcup_{s=1}^{M} \mathscr{T}_{\mathrm{FV}_s} = \Omega$, with $\mathscr{T}_{\mathrm{FE}_i} \cap \mathscr{T}_{\mathrm{FE}_j} = \emptyset$, $\mathscr{T}_{\mathrm{FV}_i} \cap \mathscr{T}_{\mathrm{FV}_j} = \emptyset$ for $i \neq j$. In our case in each FE $\mathscr{T}_{\mathrm{FE}_m}$ the unknown function $\Phi(x)$ is locally represented by $\Phi_m(x) = \sum_{k=1}^{r+1} N_k(x)\phi_k$, $N_k(x) \in \mathscr{P}_r(\hat{K})$, where $N_k(x)$ are the trial functions, $\mathscr{P}_r(\hat{K})$ is the space of polynomial forms of degree at most r on the reference element $\hat{K}$, and ϕ_k are the nodal values, providing a unique representation of the unknown variable $\Phi(x)$ all over the domain. In the finite volume element approach, the FE functional representation is used to evaluate numerical fluxes on the finite volumes boundaries. In the present approach, the set of the FE nodal values $\{\phi\}_{\hat{K}}$ in each reference element $\hat{K}$ is decomposed in the sum $\{\phi\}_{\hat{K}} = \{\overset{*}{\phi}\}_{\hat{K}} \cup \{\hat{\phi}\}_{\hat{K}}$, where $\{\hat{\phi}\}_{\hat{K}}$ is the set of the nodal values for which a FV conservation balance is present and $\{\overset{*}{\phi}\}_{\hat{K}}$ are all the remaining FE internal unknowns (see Figure 1(b)). The local FE representation inside each $\mathscr{T}_{\mathrm{FE}_m}$ can be rewritten in the following form:

$$\Phi_m(x) = \sum_{t=1}^{k_1} \hat{N}_t(x)\hat{N}_t + \sum_{s=1}^{k_2} \overset{*}{N}_s(x)\,\overset{*}{\phi}_s, \quad \text{where } k_1 + k_2 = r + 1 \tag{1}$$

By introducing a linear mapping $\mathscr{F}$ between each element $\overset{*}{\phi}_q$ of $\{\overset{*}{\phi}\}$ and a suitable subset $\{\hat{\phi}_p\}$ of $\{\hat{\phi}\}$, an explicit substitution $\overset{*}{\phi}_q = \mathscr{F}(\{\hat{\phi}_p\})$ can be obtained, resulting in an implicit coupling among all the unknowns $\{\hat{\phi}\}$ for which a FV balance is imposed. An advantage of this approach is that the increased order of accuracy of the element does not increase the number of unknowns with respect to the lower-order formulation, the latter being determined only by the nodes for which a conservation balance is present. On the other hand, depending on the functional mapping chosen between $\{\overset{*}{\phi}\}$ and $\{\hat{\phi}\}$, the structure of the final linear system changes, as the computational stencil grows as a consequence of the increasing number of the unknowns implicitly coupled each other.

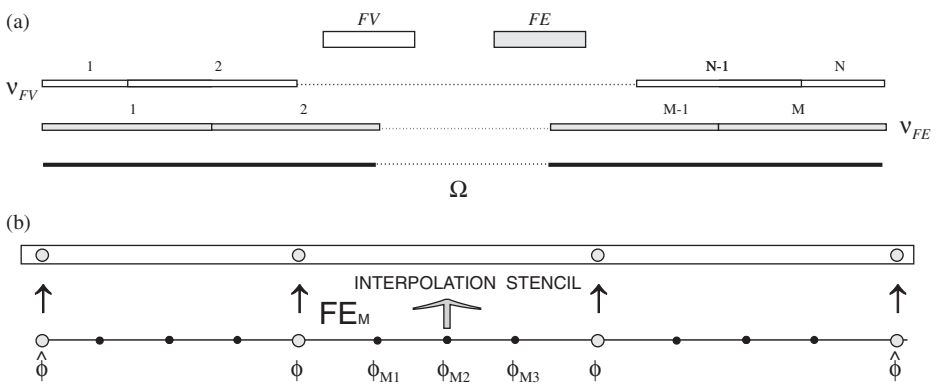

Figure 1. (a) domain Ω dual tessellation (b) FE internal $\overset{*}{\phi}$ and FV balance nodes $\hat{\phi}$.

3. 1D ADVECTION CASE

The global balance equation form for a 1D linear advective transport can be written in weak form as

$$\sum_{r=1}^{N} \int_{\mathscr{T}_{\mathrm{FV}_r}} w_r \left(\frac{\partial \phi(x,t)}{\partial t} + u \frac{\partial \phi(x,t)}{\partial x} \right) \mathrm{d}\mathscr{T}_{\mathrm{FV}_r} = 0 \tag{2}$$

where u is the velocity, assumed with constant value, $\Omega = \bigcup_{r=1}^{N} \mathscr{T}_{\mathrm{FV}_r}$, $x \in [0, L]$, $\phi_0 = \phi_L$ (periodic boundary conditions), and $\{w_r\}$ is the set of test functions, defined as

$$w_r = \begin{cases} \dfrac{1}{\mathrm{meas}(\mathscr{T}_{\mathrm{FV}_r})} & \text{if } x \in \mathscr{T}_{\mathrm{FV}_r} \\ 0 & \text{otherwise} \end{cases}$$

The choice of the mapping function $\mathscr{F}$ between internal $\{\overset{*}{\phi}\}$ and CV variables $\{\hat{\phi}\}$ is a key point of the method. In this work, compact support functions were chosen in order to reduce the size of the computational molecule for each control volume, and more precisely polynomial forms. The choice of the mapping function has a strong impact on the spectral resolution and dispersion characteristics of the scheme. In LES, for instance, centered schemes are required in order to correctly transport the resolved frequencies, while upwind schemes tend to cut the lower part of the spectrum near the cutoff frequency [23]. In order to obtain a centred computational molecule, in this work polynomial interpolation forms of odd degree are chosen: in 1D their stencil is centred with respect to the FE itself, while in the multidimensional case its support is centred with respect to the the edge of the FE where internal nodes need to be mapped. The global computational molecule obtained in this case is centred. Using the mapping function $\mathscr{F}$ between internal $\{\overset{*}{\phi}\}$ and CV variables $\{\hat{\phi}\}$, it is now possible to express Equation (2) only in term of the latter.

Introducing the finite dimensional space $\hat{V} \in \mathscr{P}_r$ of the trial functions, and the space of polynomial interpolating forms $\hat{F} \in \mathscr{P}_s$, we can now define the finite volume element (FVE)rs.

If we choose $\hat{V} \in \mathscr{P}_2(\hat{K})$ and $\hat{F} \in \mathscr{P}_3(\hat{K})$ we obtain the element FVE23 and the Equation (2) for the generic FV balance node i in the semi-discretized form can be written as

$$-\frac{1}{6}\dot{\phi}_{i-2} + \dot{\phi}_{i-1} + \frac{19}{3}\dot{\phi}_i + \dot{\phi}_{i+1} - \frac{1}{6}\dot{\phi}_{i+2} = \frac{u}{h}\left(\frac{1}{2}(\phi_{i-2} - \phi_{i+2}) + 5(\phi_{i+1} - \phi_{i-1})\right) \tag{3}$$

while using $\hat{V} \subseteq \mathscr{P}_4(\hat{K})$ and $\hat{F} \subseteq \mathscr{P}_3(\hat{K})$ (FVE43)

$$\begin{aligned}&\frac{1}{12}\left(-\frac{7}{4}\dot{\phi}_{i-2} + 11\dot{\phi}_{i-1} + \frac{155}{2}\dot{\phi}_i + 11\dot{\phi}_{i+1} - \frac{7}{4}\dot{\phi}_{i+2}\right)\\ &\quad = \frac{u}{h}\left(\frac{1}{2}(\phi_{i-2} - \phi_{i+2}) + 5(\phi_{i+1} - \phi_{i-1})\right)\end{aligned} \tag{4}$$

and using $\hat{V} \subseteq \mathscr{P}_4(\hat{K})$ and $\hat{F} \subseteq \mathscr{P}_5(\hat{K})$ (FVE45)

$$\begin{aligned}&\frac{1}{1440}\left(\frac{1303}{4}\dot{\phi}_{i-3} - \frac{4453}{2}\dot{\phi}_{i-2} + \frac{39\,257}{4}\dot{\phi}_{i-1} + 76333\dot{\phi}_i\right.\\ &\quad \left. + \frac{39\,257}{4}\dot{\phi}_{i+1} - \frac{4453}{2}\dot{\phi}_{i+2} + \frac{1303}{4}\dot{\phi}_{i+3}\right)\\ &\quad = \frac{u}{h}\left(\frac{3}{4}(\phi_{i+3} - \phi_{i-3}) + 7(\phi_{i-2} - \phi_{i+2}) + \frac{175}{4}(\phi_{i+1} - \phi_{i-1})\right)\end{aligned} \tag{5}$$

4. ERROR AND DISPERSION ANALYSIS

Assuming that the solution is smooth enough to perform an expansion in Taylor series the leading terms in the local truncation errors (LTE) for FVE23, FVE43 and FVE45 are:

$$\mathrm{LTE(FVE23)}_i \equiv -h^4\left(\frac{5}{288}\dot{\phi}^{(4)} + \frac{11}{480}\phi^{(5)}\right) + O(h^6) \tag{6}$$

$$\mathrm{LTE(FVE43)}_i \equiv -h^4\left(\frac{17}{1152}\dot{\phi}^{(4)} + \frac{11}{480}\phi^{(5)}\right) + O(h^6) \tag{7}$$

$$\mathrm{LTE(FVE45)}_i \equiv h^6\left(\frac{3493}{1\,105\,920}\dot{\phi}^{(6)} + \frac{197}{40\,320}\phi^{(7)}\right) + O(h^8) \tag{8}$$

where $\phi^{(k)} = \partial^k\phi/\partial x^k$ and $\dot{\phi} = \partial\phi/\partial t$. It is possible to demonstrate that for uniform grids the semi-discretized Equation (3) is exactly equivalent to the fourth-order Padé scheme in the FD approach at the end of the Runge-Kutta step. In order to perform Fourier analysis we consider a single Fourier mode of our initial data $\phi_0(x) = \mathrm{e}^{\mathrm{i}kx}$. Because of the periodicity

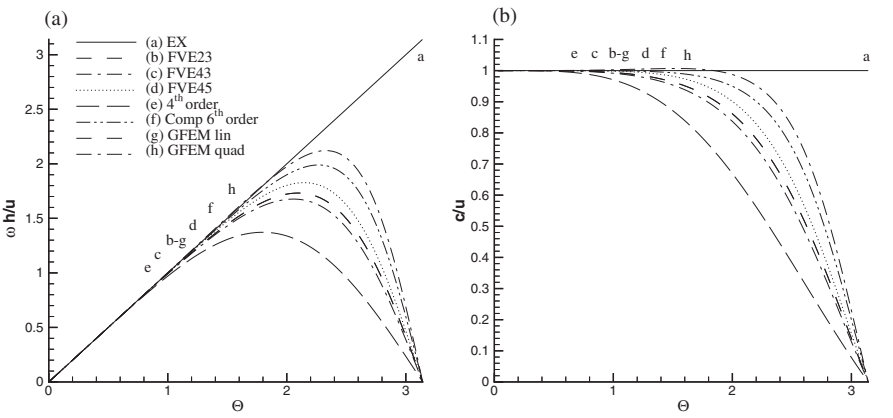

Figure 2. Eigenvalues: (a) and phase speed; (b) for pure 1D advection: (a) exact, (b) FVE23, (c) FVE43, (d) FVE45, (e) FD Fourth-order, (f) Compact Sixth-order, (g) GFEM linear, (h) GFEM quad.

constraint the wave number k can assume the values $k_n = 2\pi n$, where $n \in N_0$. The corresponding wavelength is $\lambda_n = 2\pi/k = 1/n$ and the exact solution is $\phi(x,t) = e^{i k(x-ut)} = e^{i(2\pi n x - \omega_c t)}$, where $\omega_c \equiv ku = 2\pi nu$ is the temporal frequency of the wave. Introducing a partition of Ω by means of N equispaced nodes such as $x \to x_j = jh$, the associate discrete solution is

$$\phi_j(t) = e^{i k_n jh} e^{-i\omega t} \tag{9}$$

If we define the dimensionless wave number $\theta \equiv kh$, substituting Equation (9) into the semi-discretized Equations (3)–(5) after some manipulations we obtain the modified wave numbers

$$\omega_{\mathrm{FVE23}} = 3uk \frac{10\sin(\theta) - \sin(2\theta)}{19 + 6\cos(\theta) - \cos(2\theta)} \tag{10}$$

$$\omega_{\mathrm{FVE43}} = 12uk \frac{5\sin(\theta) - \frac{1}{2}\sin(2\theta)}{\frac{155}{4} + 11\cos(\theta) - \frac{7}{4}\cos(2\theta)} \tag{11}$$

$$\omega_{\mathrm{FVE45}} = 2880uk \frac{\frac{175}{4}\sin(\theta) - 7\sin(2\theta) + \frac{3}{4}\sin(3\theta)}{76\,333 + \frac{39\,257}{2}\cos(\theta) - 4453\cos(2\theta) + \frac{1303}{2}\cos(3\theta)} \tag{12}$$

which can be compared with the exact one $\omega_c \equiv uk$. In Figure 2 the eigenvalues and the numerical phase speed are plotted with respect to the dimensionless wave number θ.

The results show that the proposed FVE method is characterized by a good resolution characteristics, although inferior at least on uniform meshes to other simpler lower order methods like quadratic Galerkin finite element method (GFEM). For resolution characteristics we mean the accuracy with which the full range of length scales that can be realized on a given mesh is represented by the discrete scheme. In this sense we can define the proposed FVE scheme a spectral-like scheme. However, these results should be considered carefully: they are obtained for uniform meshes, while on non-uniform meshes the real resolution can be quite different, as the superconvergence property of classical GFEM does not hold.

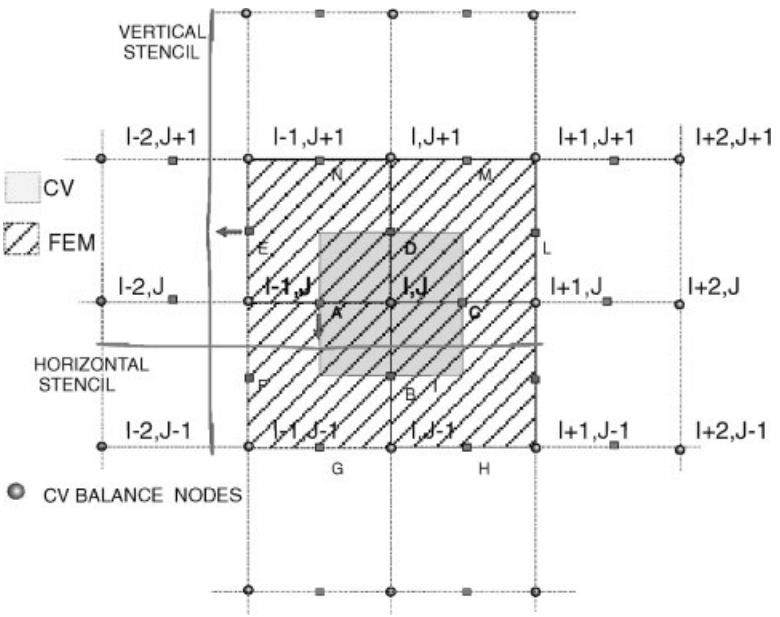

Figure 3. Computational stencil for FVE23 type.

5. EXTENSION TO MULTIDIMENSIONAL CASE

The methodological approach described above can be extended to multidimensional cases; the essential elements remain the choice of the FE trial function space and the space $\hat{F}$ of the mapping functions. If we want to retain for $\hat{F}$ the space of polynomial 1D interpolations, the extension is straightforward in the case of cartesian grids, while in the case of non-cartesian grids it requires further considerations: although it is still possible to use different mapping functions, it is out of the purpose of the present work. As a consequence, in this paper only results referring to cartesian uniform and non-uniform grids are presented. An attractive choice for the FE space is to use Serendipity elements [24, 25]; these spaces are constructed using as reference trial functions the space $S_r(\hat{K})$ which is the span of $\mathscr{P}_r(\hat{K})$ together with the two monomial $\hat{x}^r\hat{y}$ and $\hat{y}^r\hat{x}$, allowing local degrees of freedom that can be used to ensure interelement continuity. In the proposed approach quadratic (FVE2x) and quartic (FVE4x) elements, in which a central node adds a $(1-\hat{x}^2)(1-\hat{y}^2)$ shape function, are used to generate the finite volume elements FVE23 and FVE43-FVE45. In Figure 3 the complete stencil for a generic internal Finite Volume k is shown for bidimensional elements FVE23.

6. APPLICATION TO 2D ADVECTION AND ELLIPTIC PROBLEMS

6.1. 2D Convective scalar transport

Linear advective scalar transport numerical tests were performed simulating the pure advection case proposed by Casper and Atkins [26]. In this simulation a function $f(x, y, t) = 1/2(\cos(\pi(x+$

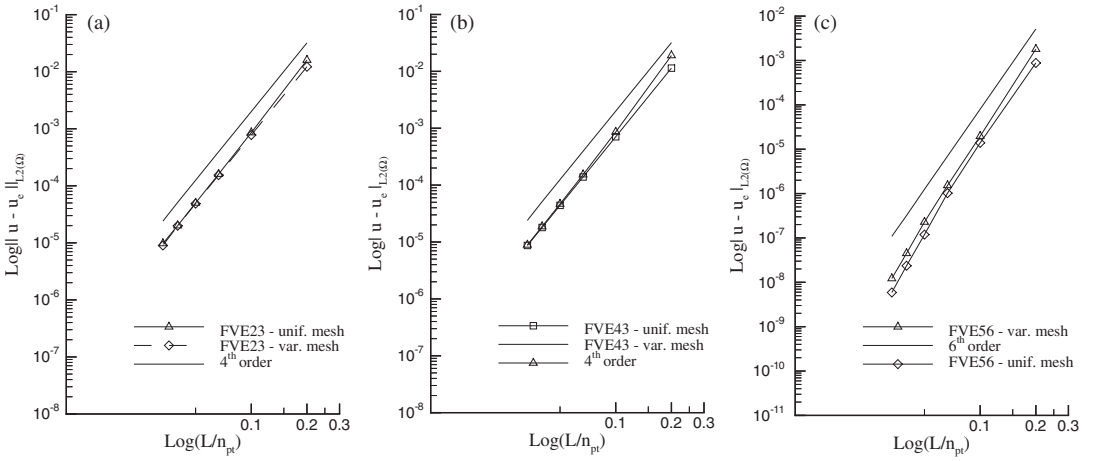

Figure 4. Linear advection 2D test: results obtained using FVE23(a), FVE43(b) and FVE45(c).

$y-2t))+1)$ at $t=0$ is advected by a diagonal vector velocity field $(u=1, v=1)$ until $t=2$ on the domain $[x, y]\in[-1,1]\times[-1,1]$. For the temporal discretization a fourth-order Runge–Kutta method was employed, and all tests were performed by using a fixed timestep Δt. The computed L_2 norm $\|\hat{u}-u_e\|_{L_2(\Omega)}$ using the numerical solution $\hat{u}$ and the exact one u_e is plotted in Figure 4 for a sequence from 10×10 to 60×60 mesh nodes and compared with the slope of different rate of accuracy for both uniform and non-uniform meshes.

6.2. 2D Elliptic problem

Numerical tests have been performed also on elliptic operators, solving a biperiodic BC problem for the Poisson equation

$$\triangle u = f \quad \text{on } \Omega \tag{13}$$

where Ω is the square $[0,2\pi]\times[0,2\pi]$. The rhs of Equation (13) f is taken so that the exact solution is

$$u(x, y) = \sin(x)\cos(2y)$$

The computed L_2 norm $\|\hat{u}-u_e\|_{L_2(\Omega)}$ is plotted in Figure 5 for a sequence from 20×20 to 80×80 mesh nodes both uniform and non-uniform meshes. Results show that while in the linear advective tests the order of accuracy is $O(h^4)$ for FVE43 and $O(h^6)$ for FVE45, here, they seem to converge with $O(h^4)$, although using the same number of points the absolute error for FVE45 is much smaller.

7. APPLICATION TO NAVIER–STOKES EQUATIONS

In order to validate the accuracy of the proposed FVE schemes, numerical tests have been performed by solving the 2D Navier–Stokes equations in the case of an incompressible flow.

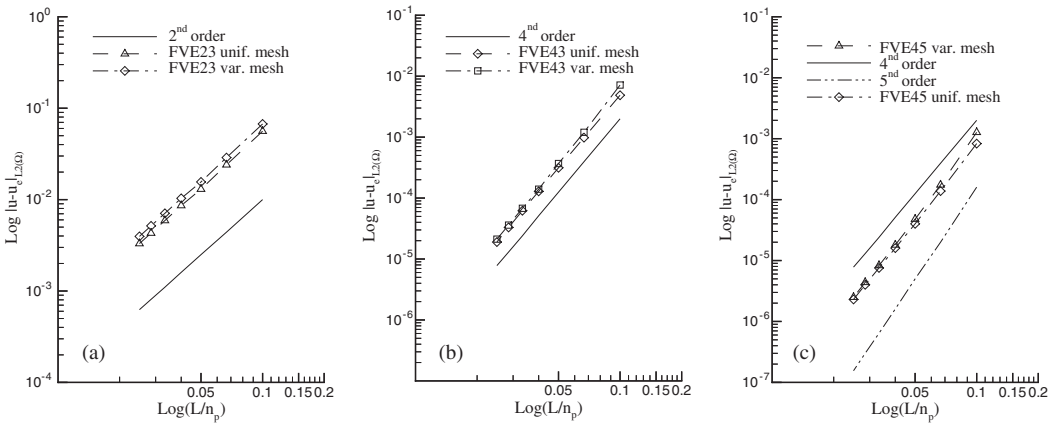

Figure 5. Poisson equation test: results obtained using FVE23(a) FVE43(b) FVE45(c).

Integrating the unsteady NS momentum equation for incompressible flows on a generic FV $\mathscr{T}_{\mathrm{FV}_i}$, and applying Gauss theorem we obtain

$$\frac{\mathrm{d}}{\mathrm{d}t}\int_{\mathscr{T}_{\mathrm{FV}_i}} \mathbf{v}\,\mathrm{d}\mathscr{T}_{\mathrm{FV}_i} + \int_{\partial\mathscr{T}_{\mathrm{FV}_i}} (\mathbf{vv})\cdot\mathbf{n}\,\mathrm{d}\partial\mathscr{T}_{\mathrm{FV}_i} = \frac{1}{Re}\int_{\partial\mathscr{T}_{\mathrm{FV}_i}} \nabla\mathbf{v}\cdot\mathbf{n}\,\mathrm{d}\partial\mathscr{T}_{\mathrm{FV}_i} - \int_{\mathscr{T}_{\mathrm{FV}_i}} \nabla P\,\mathrm{d}\mathscr{T}_{\mathrm{FV}_i} \tag{14}$$

The NS equations are solved in a collocated arrangement using a projection method on the weak integral form (14), and time integration has been performed by means of a fourth-order Runge–Kutta method. An exact solution of the two-dimensional incompressible non-steady Navier–Stokes equations is considered. The problem is assumed to be periodic in both directions x and y and therefore periodic boundary conditions have been considered. The exact solution for velocity and pressure is given by

$$u = u_0 \mathrm{e}^{-\lambda t}\sin(ax)\sin(by)$$

$$v = v_0 \mathrm{e}^{-\lambda t}\cos(ax)\cos(by)$$

$$\frac{p}{\rho} = \frac{P_0}{\rho} + \tfrac{1}{4}u_0^2\mathrm{e}^{-2\lambda t}\cos(2ax) - \tfrac{1}{4}v_0^2\mathrm{e}^{-2\lambda t}\cos(2by)$$

where u_0, v_0, p_0 and b are constants and:

$$v_0 = \frac{au_0}{b}, \quad \lambda = \nu(a^2+b^2)$$

Here $Re = 20$, $L_x = L_y = 1$ and initial condition is given by setting $t = 0$. The exact solution consists of sinusoidal waves (Taylor solution) in x and y directions which decay in time. Compared with classical FV methods, the mapping between $\{\hat{\phi}\}$ and $\{\overset{*}{\phi}\}$ at time t^{n+1} introduces an implicit character in both steps required to evaluate the provisional value $\overset{*}{\mathbf{v}}$ for the velocity and the updated values $\mathbf{v}^{n+1}$. This augmented computational weight, however, is balanced when implicit time integration is required, for example evaluating viscous fluxes like

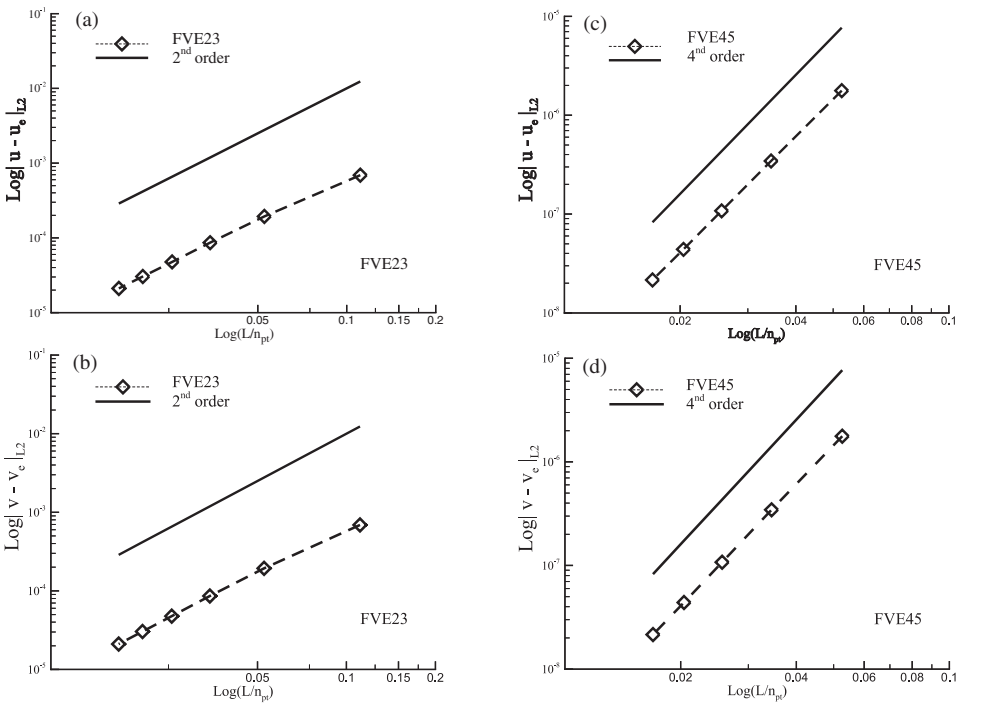

Figure 6. Taylor solution of Navier Stokes equations: L_2 norm for u-FVE23(a), v-FVE23(b),u-FVE45(c), u-FVE45(d).

in most of the cases involving the presence of wall boundaries. Results obtained in these computations show that the order of accuracy is maintained with respect to the coupling between the solution of the momentum equation for the computation of velocity $\overset{*}{\mathbf{v}}$ and the solution of the Poisson equation for the enforcement of continuity. In Figure 6 are shown the norms $\|\hat{u}-u_E\|_{L_2}$ and $\|\hat{v}-v_E\|_{L_2}$ of the u and v velocity components at $t=0.025$ respect to the mesh size for both global second- and fourth-order schemes FVE23 and FVE45.

8. CONCLUSIONS

In this paper a class of high-order FVE schemes with spectral-like spatial resolution characteristics for Navier–Stokes equations is presented. This method, targeted to applications in which low dispersion and low dissipation characteristics are required, allows a reduction of the heavy computational effort typical of higher-order finite element methods, through an implicit reduction of the number of unknowns by a local implicit mapping of some degrees of freedom, maintaining the order of accuracy, the spatial resolution and the low dispersion characteristics in both uniform and non-uniform meshes. Although numerical tests highlight the accuracy and the good spatial resolution characteristics in term of modified wave number of the proposed method, further improvements can be obtained by optimizing the class of the

mapping function $\mathscr{F}$. In this validation step, the method has been applied to cartesian variable mesh domains, but it is possible to generalize the approach on more complex geometries.

REFERENCES

1. Lele SK. Compact finite difference schemes with spectral-like resolution. *Journal of Computational Physics* 1992; **103**:16–42.
2. Chu PC, Fan C. A three-point combined compact difference Scheme. *Journal of Computational Physics* 1998; **140**:370–399.
3. Chu PC, Fan C. A three-point sixth-order nonuniform combined compact difference scheme. *Journal of Computational Physics* 1999; **148**:663–674.
4. Mahesh K. A family of high order finite difference schemes with good spectral resolution. *Journal of Computational Physics* 1998; **145**:332–358.
5. Kim JW, Lee DJ. Optimized compact finite difference schemes with maximum resolution. *AIAA Journal* 1996; **34**(5):370–399.
6. Samarskii A, Lazaroff R, Makarov L. *Finite Difference Schemes For Differential Equations with Weak Solution*. Moskow Vissaya Skola: Moskow, 1987.
7. Heinrich B. *Finite Differences Methods on Irregular Networks*. Alkademie-Verlag: Berlin, 1987.
8. Cai Z. On the finite volume element method. *Numerical Mathematics* 1991; 1992; **58**:713–735.
9. Cai Z, Mandel J, McCormick S. The finite volume element method for diffusion equations on general triangulations. *SIAM Journal of Numerical Analysis* 1991; **28**(2):392–402.
10. Süli E. In *The Mathematics of Finite Elements Methods on Distorted Partitions*, Whiteman J (ed.). Academic Press: London, 1991.
11. Morton KW, Süli E. Finite volume methods and their analysis. *IMA Journal of Numerical Analysis* 1991; **11**:241–260.
12. Eymard R, Gallouët T, Herbin R. Finite volume methods. In *Handbook of Numerical Analysis*, Ciarlet-Lions (ed.). vol. 5, 1997.
13. McCormick S. *Multilevel Adaptive Methods for Partial Differential Equations*. SIAM: Philadelphia, PA, 1989.
14. Baliga BR, Patankar SV. A new finite element formulation for convection-diffusion problems. *Numerical Heat Transfer* 1980; **3**:393–409.
15. Hookey NA, Baliga BR, Prahash C. Evaluation and enhancements of some control volume-finite element methods—Part 1. Convection–diffusion problems. *Numerical Heat Transfer* 1988; **14**:225–272.
16. Hookey NA, Baliga BR, Prahash C. Evaluation and enhancements of some control volume-finite element methods—Part 2. Incompressible fluid flow problems. *Numerical Heat Transfer* 1988; **14**:273–293.
17. Swaminathan CR, Voller VR. Streamline upwind scheme for control volume finite elements, Part 1—Formulations. *Numerical Heat Transfer*, *Part B* 1992; **22**:95–107.
18. Swaminathan CR, Voller VR. Streamline upwind scheme for control volume finite elements, Part 2—Implementation and comparison with the SUPG finite element method. *Numerical Heat Transfer*, *Part B* 1992; **22**:108–124.
19. Croisille JP. Finite volume box schemes. *2nd International Symposium on Finite Volume for Complex Applications*, Duisburg, July 99.
20. Croisille JP. Finite volume box schemes and mixed methods, *Mathematical Modeling and Numerical Analysis* 2000; **34**(5):1087–1106.
21. Lazarov JE, Pasciak PS, Vassilevski PS. Coupling mixed and finite volume discretizations of convection–diffusion–reaction equations on non-matching grids. *2nd International Symposium on Finite Volume for Complex Applications*, Duisburg, July 99.
22. Gresho PM, Sani RL. *Incompressible Flow and the Finite Element Method*. (2nd edn). Wiley: New York, April 2000.
23. Mittal R, Moin P. Suitability of upwind-biased finite difference schemes for large Eddy simulation of turbulent flows. *AIAA Journal* 1997; **35**(8):1415–1417.
24. Zienkiewicz OC, Iso-parametric and associated elements families for two and three dimensional analysis. *Finite Element Method in Stress Analysis*, Tapir Press: Norway, 1968.
25. Taylor RL. On completeness of shape function for finite element analysis. *International Journal for Numerical Method in Engineering* 1972; **4**:17–22.
26. Casper J, Atkins HL. A finite-volume high-order ENO scheme for two-dimensional hyperbolic systems. *Journal of Computational Physics* 1993; **106**:62–76.

